Plasmon-Induced Doping of Graphene

Zheyu Fang,[†,¶,#,*] Yumin Wang,[†,#] Zheng Liu,[§,#] Andrea Schlather,[†] Pulickel M. Ajayan,[§] Frank H. L. Koppens,[⊥,*] Peter Nordlander,[†,‡,*] and Naomi J. Halas[†,‡,*]

[†]Department of Electrical and Computer Engineering, Laboratory for Nanophotonics, [‡]Department of Physics and Astronomy, and [§]Mechanical Engineering and Materials Science Department, Rice University, Houston, Texas 77005, United States, [⊥]ICFO—Institut de Ciencies Fotoniques, Mediterranean Technology Park, 08860 Castelldefels, Barcelona, Spain, and [¶]School of Physics, State Key Lab for Mesoscopic Physics, Peking University, Beijing, 100871, China. [#]These authors contributed equally to this work.

ABSTRACT A metallic nanoantenna, under resonant illumination, injects nonequilibrium hot electrons into a nearby graphene structure, effectively doping the material.

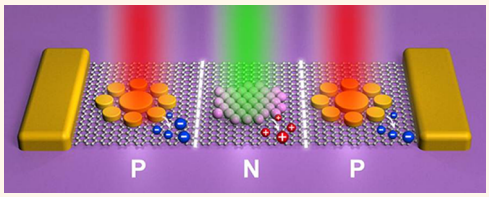

A prominent change in carrier density was observed for a plasmonic antenna-patterned graphene sheet following laser excitation, shifting the Dirac point, as determined from the gate-controlled transport characteristic. The effect is due to hot electron generation resulting from the decay of the nanoantenna plasmon following resonant excitation. The effect is highly tunable, depending on the resonant frequency of the plasmonic antenna, as well as on the incident laser power. Hot electron-doped graphene represents a new type of hybrid material that shows great promise for optoelectronic device applications.

KEYWORDS: plasmonics · graphene · hot electrons · doping · Fermi energy

Graphene, a one-atom-thick sheet of sp^2-hybridized, hexagonally arranged carbon atoms, has triggered tremendous interest due to its high electron mobility, superb mechanical flexibility, and unique optical characteristics.[1−7] Graphene-based applications such as transparent electrodes, solar cells, and ultrafast photodetectors and phototransistors have been recently demonstrated.[7−12] The linear dispersion of graphene and the absence of a bandgap, along with its unusual doping properties, make it a material of extraordinary potential for optoelectronic device applications.[1,3,13,14] In particular, photodetection based on hot carrier generation exhibits high internal quantum efficiencies.[15−17] Hot carriers have been exploited as well for some other promising applications, including graphene-based heterojunctions and bolometers.[2,18,19] Recently, light-induced carrier transfer from quantum dots to graphene was used for ultrasensitive photodetection.[20]

Metal-based subwavelength antennas, placed in direct contact with the graphene sheet, are particularly promising candidates for light-induced hot carrier injection. In the visible region of the spectrum, the optical response of these structures is dominated by the excitation of surface plasmons. Antennas consisting of an arrangement of closely spaced, coupled nanoparticles, known as plasmonic oligomers, can be designed to have large absorption cross sections in the visible range, with strong field enhancements in the gaps of the coupled nanoparticles. Some plasmonic oligomers display unique spectral lineshapes known as Fano resonances, characterized by a narrow spectral transparency window where scattering is suppressed and absorption is enhanced.[21−28] The physical origin of a plasmonic Fano resonance is a weak coupling between a spectrally broad bright superradiant plasmon mode and a spectrally narrow dark subradiant mode that does not couple directly to incident radiation. When the oligomer antenna is excited at the wavelength of the subradiant mode, light is coupled into the subradiant mode through the superradiant mode and can result in a strong indirect excitation of the subradiant mode. Since the subradiant mode is dark and does not directly couple to radiation, its dominant decay mechanism is electron−hole pair formation resulting in efficient hot electron production. Excitation of a plasmonic Fano resonance thus leads to enhanced absorption and hot electron production compared to excitation of standard bright plasmon resonances. This unique property of plasmonic Fano resonances has recently been exploited to enhance the photocurrent in plasmon based photodetectors.[29−32]

Figure 1 shows the absorption and scattering spectra of a typical Fano resonant plasmonic oligomer antenna, a nonamer consisting of eight gold disks surrounding a larger center disk. The scattering spectra exhibit a double-peaked structure consisting

* Address correspondence to zf4@rice.edu, frank.koppens@icfo.es, nordland@rice.edu, halas@rice.edu.

Received for review August 31, 2012 and accepted September 23, 2012.

Published online September 23, 2012
10.1021/nn304028b

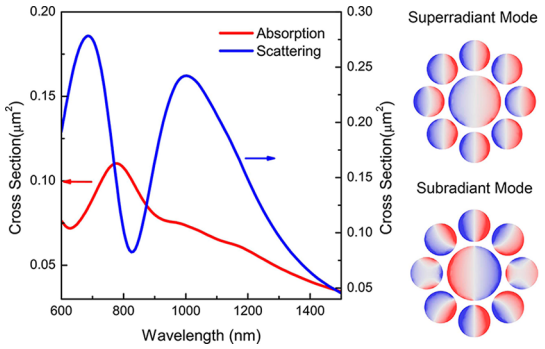

Figure 1. FDTD calculated scattering (blue) and absorption (red) spectra of a plasmonic nonamer consisting of a gold center disk of diameter 190 nm surrounded by eight gold disks of diameters 112 nm. The gap separation is 15 nm and the disk thicknesses are 30 nm. The right panel shows the charge density amplitudes for the subradiant (λ = 780 nm) and superradiant (λ = 1000 nm) modes. The light is incident perpendicularly toward the planar antenna.

of a broad featureless superradiant resonance (centered at 850 nm and extending from 500 to 1200 nm) and an antiresonance at 825 nm (caused by the destructive interference with a narrow subradiant mode at 785 nm). Without the coupling to the subradiant mode, the superradiant mode would have peaked at 850 nm. The subradiant mode is clearly visible in the absorption spectrum as a distinct peak. The slight redshift of the bottom of the antiresonance in the scattering spectrum with respect to the subradiant mode is caused by dispersive coupling and is a typical characteristic of Fano interference when the subradiant mode has a higher energy than the superradiant mode.[21−28] The charge distribution insets show the polarization of the individual nanodisks for both the subradiant and superradiant nonamer plasmon modes.

Hybrid antenna-graphene photodetectors have been realized by electron beam lithography (EBL) fabrication of plasmonic nanostructures on a graphene sheet.[33−35] In a previous publication,[33] an 800% photocurrent enhancement and an average of up to 20% internal quantum efficiency was achieved with this approach, in a sandwich graphene−antenna−graphene device geometry. The ultrathin graphene layer (0.3 nm) can structurally relax into the interparticle gap region of the plasmonic oligomer, a region of intense local fields where hot electrons (HE)[33,36,37] can directly transfer into the conduction band and be detected as an electric current.

In this article, we report a different and more general effect, the direct observation of photoinduced *n*-doping of graphene by plasmon-generated hot electrons, revealed explicitly by electrical transport measurements. We show that the degree of hot electron doping can be controlled by varying the plasmonic antenna size, incident laser wavelength, and the laser power density. Finite-difference time-domain (FDTD)

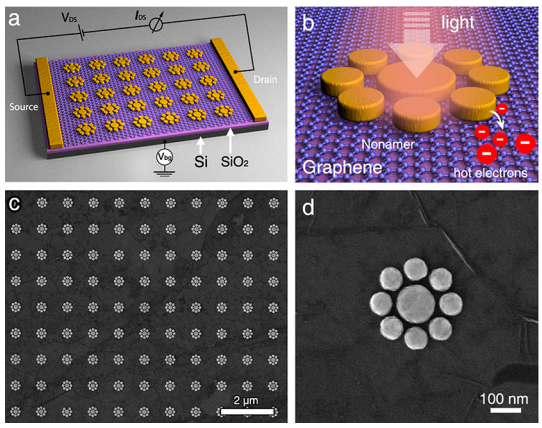

Figure 2. Plasmonic nonamer antenna-graphene phototransistor. (a) Schematic of a nonamer antenna on single-layered graphene with back-gated voltage and source and drain contacts. The device was fabricated on a Si substrate with a 285 nm thick native oxide layer. (b) Illustration of hot electron injection resulting from optically exciting the nonamer at resonance, where the plasmon decay generates hot electrons which transfer into the graphene sheet. (c) SEM image of a nonamer antenna array patterned on graphene by electron beam lithography. The diameters of the center and satellite nanodisks are 190 and 112 nm, respectively. The gap size is 15 nm. (d) SEM top view for an individual nonamer plasmonic antenna on the graphene substrate. A slight wrinkling of the graphene sheet, which occurs upon transfer to the silica substrate, is also shown.

simulations of the optical absorption spectra of the antennas are found to agree very well with the observed spectral doping profiles. The dynamic tuning of the Fermi energy in this manner provides an ultrafast and practical way to dope graphene, which can be exploited in future graphene-based optoelectronic device applications and sensors.

RESULTS AND DISCUSSION

A single graphene layer was first synthesized by chemical vapor deposition (CVD) on a copper foil, with CH_4 as the carbon source and a H_2/Ar mixture (1:5) as the carrier gas. Next, the graphene was transferred[38,39] to a silicon wafer with a 285 nm thick thermally grown native oxide layer. Using EBL and Au evaporation, source and drain electrodes and plasmonic nonamer antennas were patterned onto the monolayer graphene sheet (Figure 2a). Under laser irradiation, the hot electrons generated from plasmon excitation in the gold nonamer antennas are injected into the graphene sheets, resulting in *n*-type doping, as shown schematically in Figure 2b. SEM images of the nonamer array patterned on graphene and an individual nonamer on the graphene sheet are also shown (Figure 2c,d). The spacing of the individual nonamer antennas is 1 μm, and the diameter of the center and satellite nanodisks of each antenna are 190 and 112 nm, respectively. The gap size between individual Au nanodisks in each nonamer antenna is 15 nm. The antenna arrays were patterned in a 15 by 15 μm area between source and drain electrodes.

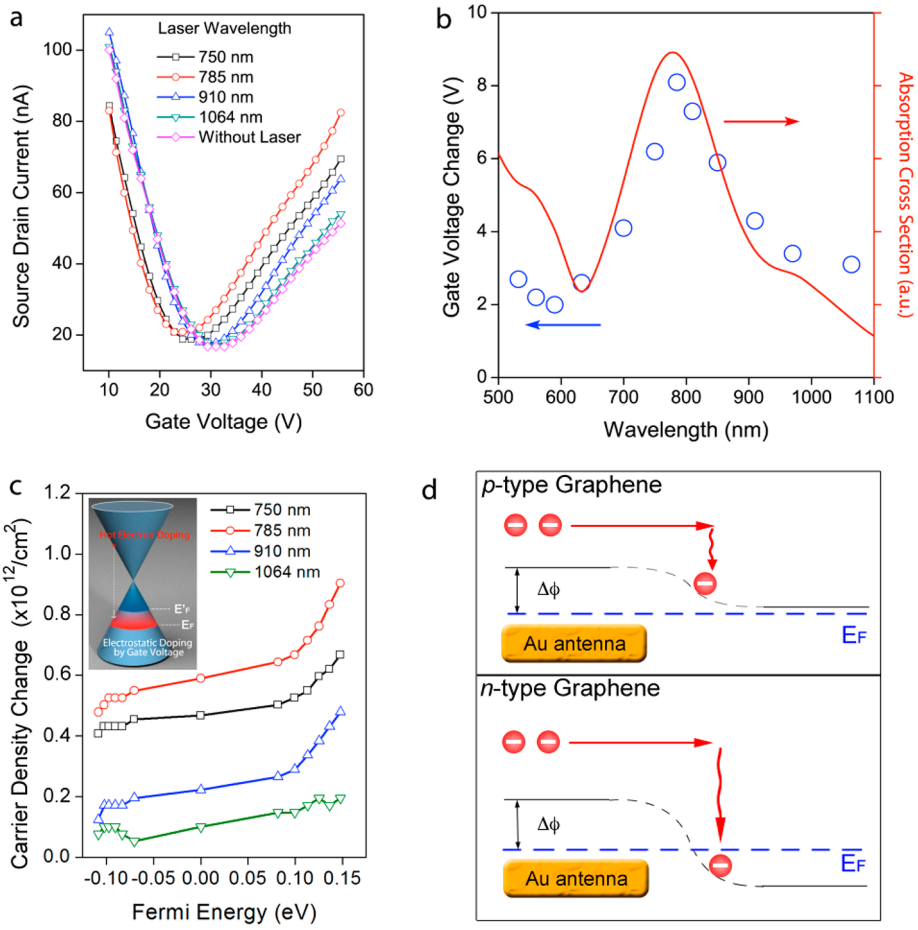

Figure 3. Dirac point shift with respect to antenna properties. (a) Electrical transport characteristic ($I-V_g$ curves) of the nonamer antenna-graphene phototransistor (size: 190 nm for diameter of central disk with 15 nm gap) measured at different incident laser wavelengths at a source−drain bias of 1 mV. (b) Blue circles: Dirac point shifts extracted from (a) under different excitation lasers with wavelengths ranging from 500 to 1100 nm (compared with the Dirac voltage for the case without laser excitation). Red curve: simulated absorption cross-section of the nonamer antenna. (c) Light-induced carrier density change with respect to Fermi energy at selectedwavelengths. Inset: Energy diagram of the graphene Dirac cone, with antenna, under laser excitation. (d) Surface potential diagram of *p*- and *n*-type graphene doped with gate voltage illustrating why photoinduced doping of *n*-type graphene is more efficient than for *p*-type.

To measure the effect of hot electrons on the electronic properties of graphene, we monitored the source−drain current of the device with respect to the backgate voltage V_g under a source−drain bias of 1 mV. The $I-V_g$ characteristic for the antenna-patterned graphene without laser excitation (the pink dotted line in Figure 3a) shows a minimum value at $V_g = V_D$ due to charge neutrality when the graphene Fermi level is at the Dirac point. In our case, $V_D \approx 30$ V, which we attribute to intrinsic doping from the SiO_2 substrate and the presence of environmental impurities (oxygen and water molecules). The equilibrium electronic structure is illustrated in the inset of Figure 3c. We use $V_g = V_D$ as the reference gate voltage in our subsequent light-induced doping experiments.

Excitation lasers with wavelengths ranging from 500 to 1100 nm were used to optically excite the nonamer antennas of our sample over this range of wavelengths. The $I-V_g$ curves show a wavelength-dependent shift of the Dirac voltage (Figure 3a). The Dirac point for all photoexcited wavelengths shift to smaller gate voltages relative to V_D. We attribute this shift to hot electron transfer to the graphene. The magnitude of the Dirac peak shift, extracted from the transport characteristics of Figure 3a, is plotted in Figure 3b as a function of incident laser wavelength. These data clearly show that the maximum shift in the Dirac point is observed for photoexcitation of the Fano resonance at 785 nm wavelength. FDTD simulations (using Johnson and Christy data) were performed to calculate the absorption cross-section of a single nonamer antenna of the same size as used in the experiment (the red line in Figure 3b). The observed consistency between simulations and experimental results shows that the wavelength-dependent shift of the Dirac point correlates well with the absorption cross-section of the antenna. This absorption cross-section determines the yield of hot electrons generated in each antenna structure.

Without laser excitation, the dopant density arising from the gate voltage can be expressed as

$n_{ES} = Q/(eA) = C_g(V_g - V_D)/(eA)$, where e is the unit charge, and C_g = *ca.* 2.4 × 10^{-14} F is the capacitance between the graphene and the back gate, which has been measured in our previous work on photodetection.[33] After the subradiant plasmons of the Au nonamer antennas are excited by laser illumination, they will decay into hot electrons which transfer to the graphene providing an additional mechanism for doping. Thus, the doping electron density can be expressed as

$$n = n_{ES} + n_{HE} = C_g(V_g - V_d)/(eA) + \tau R_{HE}/A \quad (1)$$

where R_{HE} is the rate of hot electrons generated from photon absorption in Au, and τ is the relaxation time of the optically doped carriers induced by hot electron transfer. Thus, the recorded Dirac point shift ΔV is proportional to R_{HE} and also to the absorption cross-section of the structure, $\Delta V \propto I\sigma_{abs}$, where I is the light intensity and σ_{abs} is the absorption cross-section.

By estimating the device area (A) as 200 μm^2 and the Dirac point V_D as 30 V, we can calculate the Fermi energy of graphene for each gate voltage (V_g) from the following equation, $E_F = \hbar v_F(\pi C_g(V_g - V_D)/(eA))^{1/2}$,[40−43] where v_F = 1.11 × 10^6 m S^{-1}. To extract the photogenerated change in carrier density Δn, the Dirac point difference with and without laser excitation should first be determined (Figure 3A). This is the equivalent of shifting each $I-V$ curve obtained with laser illumination to the same position on the X-axis (gate voltage) as the case without laser excitation (pink curve). Then for the source−drain current at each illumination wavelength, the gate voltage difference can be determined eq 1: the gate voltage difference is directly related to the change in carrier density induced by laser excitation. This is displayed in Figure 3c, from which we conclude that for n-type graphene ($E_F > 0$ eV), the hot electron doping efficiency is larger than for p-type graphene. When the antenna is illuminated at 785 nm, corresponding to its plasmon resonance frequency, Δn will reach a maximum value, which further proves that the nonequilibrium carrier density change depends on the absorption of the plasmonic structure.

A possible explanation for the difference in hot electron doping efficiency between p- and n-type graphene is proposed in Figure 3d. Here we show the surface potential diagram for p- and n-type graphene, taking into account the surface potential difference $\Delta\phi$ because of the work function mismatch between Au (4.7 eV) and graphene (4.5 eV). When the graphene is electrostatically p-type doped, the plasmon induced hot electrons that are injected into the graphene have a higher probability to flow back to the Au antenna and recombine with the hole, compared to the case where the graphene is electrostatically n-type doped. Possibly, this is because the photoexcited carriers have a higher probability of transmission through an ambipolar junction than through a bipolar junction.[44]

The influence of the absorption cross-section on the Dirac point shift is verified by fabricating nonamer antennas of various sizes on a graphene sheet (Figure 4). Here, the diameter of the central disk of the nonamer was varied from 170 to 270 nm (for the "without laser" case, the diameter of the central disk of the nonamer is 190 nm) and the size of the peripheral disks was also varied to maintain an interparticle gap distance of 15 nm, as in the original antenna structure. The patterned Au nanostructure can locally influence the graphene Fermi energy. However, this effect was not measured in the present experiments, since here we focus on the carrier density change following laser excitation. For each nonamer pattern, the excitation laser wavelength was carefully chosen to overlap with the dark mode frequency (Fano dip) of the structure. From the measured $I-V_g$ curves (Figure 4a), we observe that the Dirac point shift increases with increasing nonamer diameter, consistent with an increase in absorption cross-section for nanoantennas of larger and larger size.[45] Both the experiment and FDTD simulations of the absorption cross-section follow this same trend (Figure 4b). These results confirm that the observed Dirac point shift is most likely related to the plasmonic antenna absorption cross-section. They also support the conclusion that the Fermi level tuning in graphene is induced by hot electron, rather than hot hole injection: in the latter case, the Dirac point would shift to higher gate voltage values with increasing carrier density.[20]

The dependence of the Dirac point shift scales nonlinearly with incident laser power (Figure 4c). Here we excite the nonamer antenna-patterned graphene sheet at 785 nm, and vary the incident power from 0 to 50 μW. The excitation laser wavelength was chosen to be resonant with the Fano minimum of the nonamer. The dependence of the gate voltage change (ΔV) on incident laser power for p- and n-type graphene is observed (Figure 4d). For incident laser powers <5 μW, the gate voltage shifts linearly with increasing laser power. However, the power dependence becomes strongly sublinear for higher laser powers. We explain this effect as follows. As the power increases, a larger number of hot electrons are generated and injected into the graphene, which results in a larger transfer rate for hot electrons R_{HE}. However, the accumulation of positive charge in the Au antennas and negative electrons in the graphene will eventually result in an internal electrostatic field that prevents the hot electrons from leaving the antennae (see inset of Figure 4d). From the experimental data, we can further estimate our photodetector responsivity to be ~10 mA/W[1−] under 785 nm incident laser with 20 μW, which is much larger than for pristine graphene photodetection.[12,15]

The observed hot electron generation rate can be analyzed in a semiquantitative manner using data

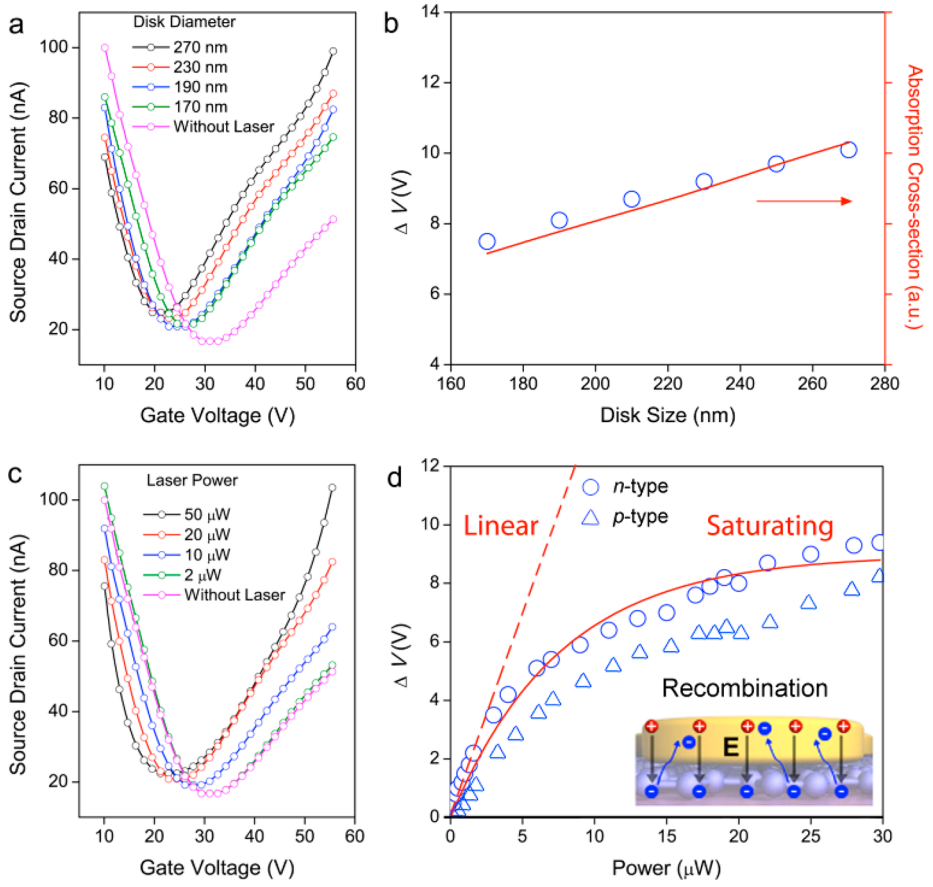

Figure 4. Dirac point shift with respect to incident laser power. (a) Electrical transport characteristic ($I-V_g$ curves) for different nonamer sizes under the same incident laser (785 nm) with a 1 mV source−drain bias. (b) Dirac point shift with different sized nonamer antennas (blue circles). Red curve: simulated absorption cross sections calculated for the size range of nonamer structures used in the experiment. (c) Electrical transport characteristic ($I-V_g$ curves) of the nonamer antenna−graphene phototransistor under different incident laser powers with a source−drain bias of 1 mV. (d) The dependence of ΔV on incident laser power for *p*- and *n*-type graphene. Inset, mechanisms for the nonlinear effect of Dirac point shift: Hot electron recombination that results from the internal electrostatic field.

measured here and also presented in our previous publication on a gold graphene photodetector.[33] From previous simulation results[33] we find most of the generated plasmonic hot electrons are transferred to the graphene. We estimate the generation rate (R_{HE}) of hot electrons for an Au nonamer antenna under a 20 μW incident power illumination to be about $\sim 4 \times 10^{11}$ s^{-1} (from ref 33). The observed dopant density (injected into *p*-type graphene) is nominally $\sim 4 \times 10^{11}$ cm^{-2} (Figure 3c), from which we can extract a relaxation time τ representing the inverse recombination rate of the hot electron-doped charge carriers. For *p*-type graphene, this time scale is nominally ~ 2 μs, while for *n*-type graphene (E_F = 0.1 eV), the dopant density of hot electrons can be as high as 6×10^{11} cm^{-2} (Figure 3c), corresponding to a τ of approximately 3 μs. This time scale estimate is rather coarse, and would require a more detailed analysis to be made more precise. In principle, we consider this microsecond time scale to be the result of three distinct processes, namely (1) the plasmonic hot electron generation rate, which is a nonequilibrium process; (2) the transfer rate for the hot electron from the Au antenna to the graphene (obtained in our previous study),[33] and (3) the injection rate of the hot electrons into the conduction band of the graphene. For a device based on this effect, the operational speed could in principle be faster than for the case of hole doping (10 ms) induced by quantum dots,[19,20] and potentially may enable very fast photodetectors with enhanced responsivity relative to pristine graphene photodetectors.

A particularly interesting concept derived from our finding of efficient photo induced doping of graphene is the possibility of generating what we will refer to as optically induced electronics (OIE). While the present plasmon induced hot electron injection results in n-doping, this process could be combined with the recently observed p-doping process observed when a graphene sheet is covered by a thin layer of quantum dots.[20] By patterning distinct regions of an undoped graphene structure with plasmonic antennas or quantum dots tuned to different (or the same) wavelength and then illuminating by light, it might be possible to create pn junctions and realize simple electronic

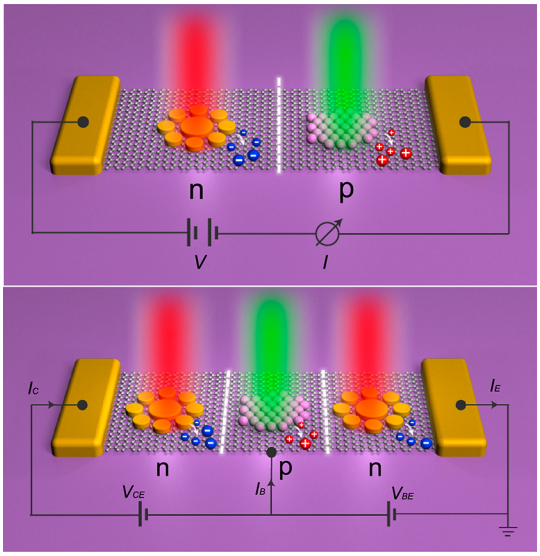

Figure 5. Schematic illustration of optically induced electronics (OIE) made possible by nanoantenna n-doping and quantum dot p-doping, inducing (top) a diode or (bottom) an npn transistor, respectively. Different regions of the undoped graphene structures are covered by either plasmonic antennas (tuned to red) or quantum dots (tuned to green). When a specific pattern of light at the requisite wavelengths illuminates the structure, HE from the plasmonic antennas induce n-doping and the holes injected from the quantum dots induce p-doping. Since the optical response of the plasmonic antennas and the quantum dots can be tuned, a similar effect could also be generated using light of the same color.

circuitry. In Figure 5, we schematically illustrate how OIE could be used to create an elementary diode or transistor. By using more complicated patterns, it may be possible to create simple electronic circuits that would turn on *only* when illuminated by an appropriate unique light pattern. Since the highly tunable characteristics of plasmonic and excitonic nanostructures also include polarization and chiral response and incidence angle, the antennas could also be tuned to induce electronic circuits upon illumination with, for example, a specific polarization state of the incident light or incidence angle. Although we foresee several experimental challenges before such a device could be realized, such as the need to localize the photoinduced carriers to the appropriate spatial regions of the pattern, OIE may find important applications in cryptography, electronic password, or counterfeit verification applications where only the specific illumination condition would activate an electrical response.

CONCLUSIONS

We have demonstrated photoinduced doping of graphene by hot electrons generated from plasmonic nanoantennas, observed electrically as a shift of the Dirac point. We have demonstrated control of this process with plasmonic antennas of various sizes with tunable plasmon resonances and a range of incident light intensities. A larger doping efficiency is achieved for the *n*-type graphene in comparison with *p*-type graphene. In addition, our microsecond doped carrier relaxation time scale could enable the development of a wide variety of active optical and optoelectronic applications, such as graphene switches and photodetectors and optically induced electronics.

METHODS

In the experiment, source–drain electrodes and plasmonic nonamer nanoantenna patterns were first fabricated on a graphene substrate by using two-step E-beam lithography and subsequent lift-off. The graphene sheet placed atop the nonamer was observed in the scanning electron microscope image of the device structure. The dependence of source–drain current on gate voltage measurements were performed using a four-probe station at a vacuum of $\sim 10^{-5}$ Torr. Incident laser with different incident wavelength and power were applied to realize the active control of optical induced graphene carried density change.

Conflict of Interest: The authors declare no competing financial interest.

Acknowledgment. Z.F., Y.W., A.S., P.N., and N.J.H. are supported by the Robert A. Welch Foundation (C-1220 and C-1222), the Office of Naval Research (N00014-10-1-0989), and the DoD NSSEFF (N00244-09-1-0067); P.M.A. and Z.L. are supported by the office of Naval Research through the MURI program on graphene. F.H.L.K is supported by Fundacio Cellex Barcelona.

REFERENCES AND NOTES

1. Bonaccorso, F.; Sun, Z.; Hasan, T.; Ferrari, A. C. Graphene Photonics and Optoelectronics. *Nat. Photonics* **2010**, *4*, 611–622.
2. Zhang, Y. B.; Tang, T. T.; Girit, C.; Hao, Z.; Martin, M. C.; Zettl, A.; Crommie, M. F.; Shen, Y. R.; Wang, F. Direct Observation of a Widely Tunable Bandgap in Bilayer Graphene. *Nature* **2009**, *459*, 820–823.
3. Castro Neto, A. H.; Guinea, F.; Peres, N. M. R.; Novoselov, K. S.; Geim, A. K. The Electronic Properties of Graphene. *Rev. Mod. Phys.* **2009**, *81*, 109–162.
4. Lin, Y. M.; Dimitrakopoulos, C.; Jenkins, K. A.; Farmer, D. B.; Chiu, H. Y.; Grill, A.; Avouris, P. 100-GHz Transistors from Wafer-Scale Epitaxial Graphene. *Science* **2010**, *327*, 662–662.
5. Novoselov, K. S.; Geim, A. K.; Morozov, S. V.; Jiang, D.; Zhang, Y.; Dubonos, S. V.; Grigorieva, I. V.; Firsov, A. A. Electric Field Effect in Atomically Thin Carbon Films. *Science* **2004**, *306*, 666–669.
6. Vakil, A.; Engheta, N. Transformation Optics Using Graphene. *Science* **2011**, *332*, 1291–1294.
7. Chen, J. N.; Badioli, M.; Alonso-Gonzalez, P.; Thongrattanasiri, S.; Huth, F.; Osmond, J.; Spasenovic, M.; Centeno, A.; Pesquera, A.; Godignon, P.; *et al.* Optical Nano-imaging of Gate-Tunable Graphene Plasmons. *Nature* **2012**, *487*, 77–81.
8. Wu, Y. Q.; Jenkins, K. A.; Valdes-Garcia, A.; Farmer, D. B.; Zhu, Y.; Bol, A. A.; Dimitrakopoulos, C.; Zhu, W. J.; Xia, F. N.; Avouris, P.; *et al.* State-of-the-Art Graphene High-Frequency Electronics. *Nano Lett.* **2012**, *12*, 3062–3067.
9. Xia, F. N.; Perebeinos, V.; Lin, Y. M.; Wu, Y. Q.; Avouris, P. The Origins and Limits of Metal-Graphene Junction Resistance. *Nat. Nanotechnol.* **2011**, *6*, 179–184.

10. Ju, L.; Geng, B. S.; Horng, J.; Girit, C.; Martin, M.; Hao, Z.; Bechtel, H. A.; Liang, X. G.; Zettl, A.; Shen, Y. R.; *et al*. Graphene Plasmonics for Tunable Terahertz Metamaterials. *Nat. Nanotechnol.* **2011**, *6*, 630–634.
11. Wang, X.; Zhi, L. J.; Mullen, K. Transparent, Conductive Graphene Electrodes for Dye-Sensitized Solar Cells. *Nano Lett.* **2008**, *8*, 323–327.
12. Xia, F. N.; Mueller, T.; Lin, Y. M.; Valdes-Garcia, A.; Avouris, P. Ultrafast Graphene Photodetector. *Nat. Nanotechnol.* **2009**, *4*, 839–843.
13. Wu, Y. Q.; Lin, Y. M.; Bol, A. A.; Jenkins, K. A.; Xia, F. N.; Farmer, D. B.; Zhu, Y.; Avouris, P. High-frequency, Scaled Graphene Transistors on Diamond-like Carbon. *Nature* **2011**, *472*, 74–78.
14. Crowther, A. C.; Ghassaei, A.; Jung, N.; Brus, L. E. Strong Charge-Transfer Doping of 1 to 10 Layer Graphene by NO_2. *ACS Nano* **2012**, *6*, 1865–1875.
15. Lemme, M. C.; Koppens, F. H. L.; Falk, A. L.; Rudner, M. S.; Park, H.; Levitov, L. S.; Marcus, C. M. Gate-Activated Photoresponse in a Graphene p−n Junction. *Nano Lett.* **2011**, *11*, 4134–4137.
16. Song, J. C. W.; Rudner, M. S.; Marcus, C. M.; Levitov, L. S. Hot Carrier Transport and Photocurrent Response in Graphene. *Nano Lett.* **2011**, *11*, 4688–4692.
17. Gabor, N. M.; Song, J. C. W.; Ma, Q.; Nair, N. L.; Taychatanapat, T.; Watanabe, K.; Taniguchi, T.; Levitov, L. S.; Jarillo-Herrero, P. Hot Carrier-Assisted Intrinsic Photoresponse in Graphene. *Science* **2011**, *334*, 648–652.
18. Liu, M.; Yin, X. B.; Ulin-Avila, E.; Geng, B. S.; Zentgraf, T.; Ju, L.; Wang, F.; Zhang, X. A Graphene-Based Broadband Optical Modulator. *Nature* **2011**, *474*, 64–67.
19. Wang, F.; Zhang, Y. B.; Tian, C. S.; Girit, C.; Zettl, A.; Crommie, M.; Shen, Y. R. Gate-Variable Optical Transitions in Graphene. *Science* **2008**, *320*, 206–209.
20. Konstantatos, G.; Badioli, M.; Gaudreau, L.; Osmond, J.; Bernechea, M.; de Arquer, F. P. G.; Gatti, F.; Koppens, F. H. L. Hybrid Graphene-Quantum Dot Phototransistors with Ultrahigh Gain. *Nat. Nanotechnol.* **2012**, *7*, 363–368.
21. Fu, Y. H.; Zhang, J. B.; Yu, Y. F.; Luk'yanchuk, B. Generating and Manipulating Higher Order Fano Resonances in Dual-Disk Ring Plasmonic Nanostructures. *ACS Nano* **2012**, *6*, 5130–5137.
22. Pasquale, A. J.; Reinhard, B. M.; Dal Negro, L. Concentric Necklace Nanolenses for Optical Near-Field Focusing and Enhancement. *ACS Nano* **2012**, *6*, 4341–4348.
23. Cui, Y. H.; Zhou, J. H.; Tamma, V. A.; Park, W. Dynamic Tuning and Symmetry Lowering of Fano Resonance in Plasmonic Nanostructure. *ACS Nano* **2012**, *6*, 2385–2393.
24. Francescato, Y.; Giannini, V.; Maier, S. A. Plasmonic Systems Unveiled by Fano Resonances. *ACS Nano* **2012**, *6*, 1830–1838.
25. Cataldo, S.; Zhao, J.; Neubrech, F.; Frank, B.; Zhang, C. J.; Braun, P. V.; Giessen, H. Hole-Mask Colloidal Nano Lithography for Large-Area Low-Cost Metamaterials and Antenna-Assisted Surface-Enhanced Infrared Absorption Substrates. *ACS Nano* **2012**, *6*, 979–985.
26. Zhao, J.; Frank, B.; Burger, S.; Giessen, H. Large-Area High-Quality Plasmonic Oligomers Fabricated by Angle-Controlled Colloidal Nanolithography. *ACS Nano* **2011**, *5*, 9009–9016.
27. Gallinet, B.; Martin, O. J. F. Influence of Electromagnetic Interactions on the Line Shape of Plasmonic Fano Resonances. *ACS Nano* **2011**, *5*, 8999–9008.
28. Dregely, D.; Hentschel, M.; Giessen, H. Excitation and Tuning of Higher-Order Fano Resonances in Plasmonic Oligomer Clusters. *ACS Nano* **2011**, *5*, 8202–8211.
29. Halas, N. J.; Lal, S.; Chang, W. S.; Link, S.; Nordlander, P. Plasmons in Strongly Coupled Metallic Nanostructures. *Chem. Rev.* **2011**, *111*, 3913–3961.
30. Luk'yanchuk, B.; Zheludev, N. I.; Maier, S. A.; Halas, N. J.; Nordlander, P.; Giessen, H.; Chong, C. T. The Fano Resonance in Plasmonic Nanostructures and Metamaterials. *Nat. Mater.* **2010**, *9*, 707–715.
31. Fan, J. A.; Wu, C. H.; Bao, K.; Bao, J. M.; Bardhan, R.; Halas, N. J.; Manoharan, V. N.; Nordlander, P.; Shvets, G.; Capasso, F. Self-Assembled Plasmonic Nanoparticle Clusters. *Science* **2010**, *328*, 1135–1138.
32. Moskovits, M. Hot Electrons Cross Boundaries. *Science* **2011**, *332*, 676–677.
33. Fang, Z. Y.; Liu, Z.; Wang, Y. M.; Ajayan, P. M.; Nordlander, P.; Halas, N. J. Graphene-Antenna Sandwich Photodetector. *Nano Lett.* **2012**, *12*, 3808–3813.
34. Echtermeyer, T. J.; Britnell, L.; Jasnos, P. K.; Lombardo, A.; Gorbachev, R. V.; Grigorenko, A. N.; Geim, A. K.; Ferrari, A. C.; Novoselov, K. S. Strong Plasmonic Enhancement of Photovoltage in Graphene. *Nat. Commun.* **2011**, *2*, 458.
35. Liu, Y.; Cheng, R.; Liao, L.; Zhou, H. L.; Bai, J. W.; Liu, G.; Liu, L. X.; Huang, Y.; Duan, X. F. Plasmon Resonance Enhanced Multicolour Photodetection by Graphene. *Nat. Commun.* **2011**, *2*, 579.
36. Stockman, M. I. Nanoscience Dark-Hot Resonances. *Nature* **2010**, *467*, 541–542.
37. Knight, M. W.; Sobhani, H.; Nordlander, P.; Halas, N. J. Photodetection with Active Optical Antennas. *Science* **2011**, *332*, 702–704.
38. Schwierz, F. Graphene Transistors. *Nat. Nanotechnol.* **2010**, *5*, 487–496.
39. Li, X. S.; Cai, W. W.; An, J. H.; Kim, S.; Nah, J.; Yang, D. X.; Piner, R.; Velamakanni, A.; Jung, I.; Tutuc, E.; *et al*. Large-Area Synthesis of High-Quality and Uniform Graphene Films on Copper Foils. *Science* **2009**, *324*, 1312–1314.
40. Koppens, F. H. L.; Chang, D. E.; de Abajo, F. J. G. Graphene Plasmonics: A Platform for Strong Light-Matter Interactions. *Nano Lett.* **2011**, *11*, 3370–3377.
41. Christensen, J.; Manjavacas, A.; Thongrattanasiri, S.; Koppens, F. H. L.; de Abajo, F. J. G. Graphene Plasmon Waveguiding and Hybridization in Individual and Paired Nanoribbons. *ACS Nano* **2012**, *6*, 431–440.
42. Manjavacas, A.; Nordlander, P.; de Abajo, F. J. G. Plasmon Blockade in Nanostructured Graphene. *ACS Nano* **2012**, *6*, 1724–1731.
43. Thongrattanasiri, S.; Koppens, F. H. L.; de Abajo, F. J. G. Complete Optical Absorption in Periodically Patterned Graphene. *Phys. Rev. Lett.* **2012**, *108*, 047401.
44. Stander, N.; Huard, B.; Goldhaber-Gordon, D. Evidence for Klein Tunneling in Graphene p−n Junctions. *Phys. Rev. Lett.* **2009**, *102*, 026807.
45. van der Hulst, H. C. *Light Scattering by Small Particles*; Dover Publications: New York, 1981.